



ELSEVIER

Progress in Surface Science 74 (2003) 319–329

Progress in
SURFACE
SCIENCE

www.elsevier.com/locate/progsurf

High-resolution electron-energy-loss spectroscopy of surface and interface phonons in multilayered materials

J.L. Guyaux^a, Ph. Lambin^{b,*}, P.A. Thiry^b

^a *Addon SA, 19 Rue des Entrepreneurs, F78420 Carrières sur Seine, France*

^b *Département de physique et Chimie, Facultés Universitaires Notre-Dame de la Paix, 61 Rue de Bruxelles, B 5000 Namur, Belgium*

Abstract

Long-wavelength surface and interface phonons have been investigated by high-resolution electron-energy-loss spectroscopy (HREELS) in two heterostructures grown by molecular-beam epitaxy. The first system is a CaF_2 insulating layer on $\text{Si}(1\ 1\ 1)$, while the second consists of GaAs/AlAs superlattices grown on a thick $\text{GaAs}(0\ 0\ 1)$ substrate. The HREELS experimental results are successfully explained by the dielectric theory, with some refinements brought about by lattice dynamics calculations.

© 2003 Elsevier Ltd. All rights reserved.

Keywords: Superlattice; Heterostructure; Interface; Phonon; EELS; HREELS; Electrostatics; Dielectric theory

1. Introduction

Heterostructures are artificial materials of great interest in today's technology [1] that have numerous applications in both fundamental research and in advanced devices [2], among which long-wavelength optoelectronic devices, quantum-well lasers, solar cells, Bragg reflectors, gas photodetectors ... [3]. Some of these applications demand a well-controlled arrangement of the successive layers and require a precise control—at the atomic scale—of the thickness of layers. It is therefore important to have reliable characterization tools to investigate the growth mechanism

* Corresponding author. Tel.: +32-81-724-710; fax: +32-81-724-707.

E-mail address: philippe.lambin@fundp.ac.be (Ph. Lambin).

and to check both the quality of the layers and the sharpness of the interfaces between them. High-resolution electron-energy-loss spectroscopy (HREELS) in reflection geometry is one of the techniques that can be used for these purposes [4]. The aim of this paper is to illustrate the ability of HREELS to probe long-wavelength surface and interface phonons in multilayered materials. After a brief account of the dielectric theory, of relevance for the interpretation of HREELS spectra taken in near-specular geometry [5], two systems are analyzed in some details. CaF_2/Si is considered as the first simple example and has attracted considerable attention, as a prototype of a well-controlled insulator/semiconductor interface, since the 1980s [6]. Next, HREELS spectra of superlattices made of very thin alternating layers of GaAs and AlAs are analyzed. The confinement of optical phonons in AlAs and GaAs layers is an interesting physical phenomenon taking place in these heterostructures [7,8]. It is shown that optical-phonon confinement has sizable effects on the HREELS spectra of the superlattice.

2. Computing the HREELS spectrum

Since the original work of Ibach on ZnO [9], HREELS in reflection geometry has emerged as a powerful tool for the study of surface vibrational modes of crystalline materials [10]. In specular geometry, HREELS probes long-wavelength vibrational or electronic excitations of the target material, which generate a macroscopic electric field outside the target. An impinging electron interacts with those modes through its Coulomb field. In general, the surface excitations of a planar material, supposed to be periodic in the directions x and y parallel to the surface, have a dispersion in the space spanned the two-dimensional surface wave vectors \vec{Q} . A planar system can be characterized by a surface-dielectric-response function in this two-dimensional reciprocal space, $g(\vec{Q}, \omega)$. By definition, this quantity gives the amplitude of the induced potential at a distance large on the atomic scale from the surface, when the system is excited by an external plane-wave potential [11].

In the classical theory of HREELS, the loss spectrum depends on g through the expression [12]

$$P_{\text{cl}}(\omega) = \frac{2}{\pi^2} \frac{e^2}{4\pi\epsilon_0\hbar v_{\perp}} \int_D \frac{Q v_{\perp}^3}{[(\vec{Q} \cdot \vec{v}_{\parallel} - \omega)^2 + (Q v_{\perp})^2]^2} \text{Im}[g(\vec{Q}, \omega)] d^2 Q, \quad (1)$$

where D is a domain of wave vectors that, according to total energy and parallel momentum conservation laws, scatter the electron into the acceptance angle of the spectrometer [13,14]. In (1), \vec{v}_{\parallel} and v_{\perp} are the components of the electron velocity parallel and perpendicular to the surface, respectively. It is supposed that the electron is moving along a rectilinear, specularly reflected trajectory. The surface modes that are excited by the electrons correspond to the poles of $g(\vec{Q}, \omega)$, which are called Fuchs–Kliwer (FK) surface modes [15], that are combinations of long-wavelength optical phonons perturbed by the surface of the target material.

By treating the surface modes as harmonic oscillators, multiple-scattering interactions with the probing electrons can be accounted for [5]. An electron is treated as a point charge moving along its classical, specularly reflected trajectory. It is supposed that the oscillators are in thermal equilibrium at the temperature of the target long before their interaction with the passing electrons. During the interaction process, a moving electron can excite an oscillator from one level to another separated by one, two ... quanta of energy. After having interacted with the FK modes, the electron will have lost equivalent amounts of energy corresponding to the emission of one, two ... surface excitations. Energy-loss peaks are observed at these positions. Similarly, electron energy gain peaks correspond to de-excitations events from thermally excited FK modes. This semi-classical theory of EELS is consistent with a full quantum-mechanical treatment of the electron surface inelastic scattering by long-wavelength optical phonons [16,17].

The total loss spectrum, which incorporates now multiple loss and gain peaks, can be written as the Fourier transform [5]

$$P(\omega) = \frac{1}{2\pi} \int_{-\infty}^{+\infty} F(\tau) e^{i\omega\tau} d\tau \quad (2)$$

of the characteristic function

$$F(\tau) = \exp \left\{ - \int_0^{+\infty} P_{cl}(\omega) \coth \frac{\hbar\omega}{2k_B T} [1 - \cos(\omega\tau)] d\omega \right. \\ \left. - i \int_0^{+\infty} P_{cl}(\omega) \sin(\omega\tau) d\omega \right\}. \quad (3)$$

Here, T is the temperature of the target and P_{cl} is the classical loss spectrum given by (1). The characteristic function $F(\tau)$ can be multiplied by the Fourier transform of an instrumental transfer function, in order to simulate the finite resolution of the spectrometer by a convolution [18]. A spectrum computed from (2) can then be directly compared to experiment. In the above derivation, the cut-off wave-vector, imposed by the spectrometer aperture has been neglected. In fact, spectrometer acceptance effects are correctly taken into account for single-scattering events (see (1)). Restricting these effects to one-phonon losses only is not fully correct [19], but the incorrectness of the procedure is generally below the experimental uncertainties.

3. The surface loss function

Microscopic calculations can be used to obtain the surface-response function g of the electron gas in a metal (by density functional theory [20]) or the response of optical phonons in a film (by lattice dynamics [21]). When the target material is treated as a continuous medium, g can be obtained from electrostatics in the form

$$g(\vec{Q}, \omega) = \frac{\xi(\vec{Q}, \omega) - 1}{\xi(\vec{Q}, \omega) + 1}, \quad (4)$$

where ξ is an effective surface-dielectric function of the system, whose definition can be found in [22]. As mentioned above, the FK surface modes of the system correspond to poles of $g(\vec{Q}, \omega)$, which means $\xi(\vec{Q}, \omega) = -1$. ξ reduces to the bulk dielectric function $\epsilon(\omega)$ of the target system in the case of a thick, isotropic medium.

The most general planar system that can be handled by the dielectric theory is an heterostructure made of a stacking of layers separated by sharp interfaces parallel to the surface. In the electrostatic approximation, valid at the long-wavelength limit, the effective surface-dielectric function of the multilayer can be written in the form of a continued fraction [22]

$$\xi = a_1 - \frac{b_1^2}{a_1 + a_2 - \frac{b_2^2}{a_2 + \ddots}} \quad (5)$$

with coefficients

$$a_j = \epsilon_j(\omega) / \tanh(Qd_j), \quad (6)$$

$$b_j = \epsilon_j(\omega) / \sinh(Qd_j), \quad (7)$$

j labelling the successive layers starting from the surface layer ($j = 1$), d_j being the thickness and ϵ_j the bulk dielectric function of the j th layer.

4. Two-layer system

For a two-layer system, with isotropic dielectric functions, the effective surface-dielectric function (5) simplifies into [23]

$$\xi = \epsilon_1(\omega) \frac{\epsilon_1(\omega) \tanh(Qd_1) + \epsilon_2(\omega)}{\epsilon_2(\omega) \tanh(Qd_1) + \epsilon_1(\omega)}. \quad (8)$$

Several branches of FK phonons exist for the present problem. By definition, *surface* modes have dispersion relations $\omega(Q)$ that converge to the solutions of $\epsilon_1(\omega) + 1 = 0$ for large Q , whereas the frequencies of the *interface* modes converge to the solutions of the relation $\epsilon_1(\omega) + \epsilon_2(\omega) = 0$. Both surface and interface modes contribute to the EELS spectrum of the target with, however, increasing weight on the surface modes, as the thickness of the topmost layer increases.

The case of a CaF_2 dielectric layer deposited on $\text{Si}(111)$ is considered as a first example [24]. The left-hand panel of Fig. 1 shows the dispersion curves of the FK phonons of a system composed of a CaF_2 layer on Si, plotted against Qd_1 . Here, the substrate (silicon) is inactive in the infrared; its dielectric function is a constant taken equal to 12 in the calculations. In this particular example, there is one surface FK branch and one interface branch, both being situated in the interval defined by the long-wavelength transverse optical ($\omega_{\text{TO}} = 257 \text{ cm}^{-1}$) and longitudinal optical ($\omega_{\text{LO}} = 460 \text{ cm}^{-1}$) phonons of CaF_2 . In the calculations, the dielectric function of CaF_2 is described with the usual Lorentzian model

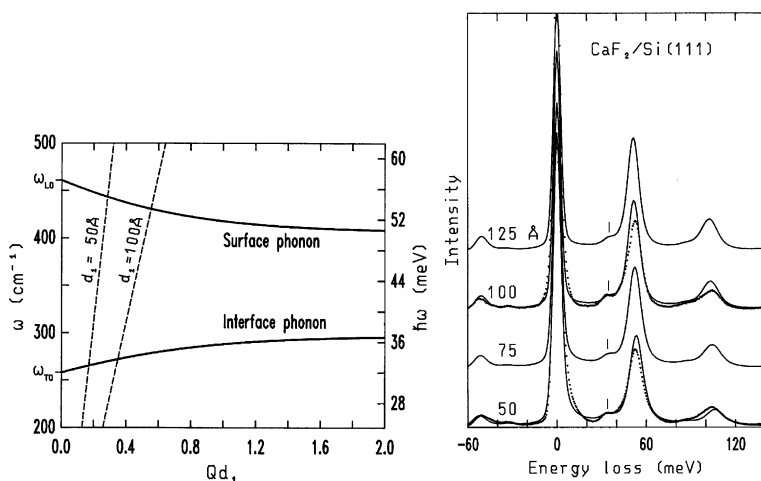


Fig. 1. Left: dispersion curves of FK phonons of CaF_2/Si versus Qd_1 , where Q is phonon wave-vector and d_1 is thickness of overlayer. Dashed lines correspond to maxima of inelastic cross section. Right: experimental (dots) and computed (solid line) EELS spectra of $\text{CaF}_2/\text{Si}(111)$ for $d_1 = 5, 7.5, 10$, and 12.5 nm. Electron energy is 6.1 eV with incidence angle of 45° .

$$\epsilon(\omega) = \epsilon(\infty) + \frac{\Delta\epsilon\omega_{\text{TO}}^2}{\omega_{\text{TO}}^2 - \omega^2 - i\gamma\omega}, \quad (9)$$

where $\Delta\epsilon = \epsilon(0) - \epsilon(\infty)$ is the difference between the static and optical-frequency dielectric constants (6.7 and 2.04 , respectively), γ is a damping constant. The dashed lines $\omega = Qv$ in Fig. 1 represent regions of the (Q, ω) plane, where the kinematic factor in the integrand of (1) is close to a maximum for the incident electron energy of 6.1 eV used experimentally. HREELS spectra, both experimental (dots) and theoretical (solid lines) are shown in the right-hand side of the figure for the same system for four values of the thickness d_1 of the CaF_2 overlayer. The prominent peak, centered around 54 meV, and its multiple loss and gain replicas are due to the surface phonon. The interface mode appears as a shoulder marked by a vertical bar at lower frequency. The dispersion of the surface and interface modes upon increasing thickness can easily be observed in the spectra. The agreement between theory and experiment is not perfect, however, especially on the peak intensities. The disagreement is due to the strain induced in the film by the lattice mismatch between $\text{Si}(111)$ and CaF_2 and to the lack of crystalline quality of the interface [24].

5. GaAs/AlAs heterostructures

GaAs/AlAs multilayers were grown on a GaAs(001) substrate by molecular-beam epitaxy (MBE). The substrate was prepared by standard etching procedure before being loaded into ultra-high vacuum. A thick GaAs buffer layer was grown at

Table 1

Dielectric constants of AlAs and GaAs (see (9))

| | ω_{TO} (cm ⁻¹) | ω_{LO} (cm ⁻¹) | $\epsilon(0)$ | $\epsilon(\infty)$ | $\Delta\epsilon$ | γ (cm ⁻¹) |
|------|--|--|---------------|--------------------|------------------|------------------------------|
| AlAs | 360 | 399.3 | 10.04 | 8.16 | 1.88 | 0.015 |
| GaAs | 267 | 290.6 | 12.91 | 10.9 | 2.01 | 0.020 |

580 °C on As-rich stabilized surface. Subsequent AlAs and GaAs epitaxial layers were grown, the thickness of which was measured by counting the number of RHEED oscillations. The lattice parameters a_0 of bulk AlAs and GaAs are very similar, 5.661 and 5.653 Å, respectively. For AlAs/GaAs multilayers grown along the [001] direction, a monolayer of each of these materials corresponds to a thickness of $a_0/2 = 2.83$ Å.

Superlattices of the form $(\text{GaAs}_n/\text{AlAs}_m)_p/\text{GaAs}(001)$ were realized with different values of n , m , and p . HREELS spectroscopy was applied to study the structure of the FK phonons in these multilayers. The HREELS spectra were compared to simulations obtained with the semi-classical dielectric theory described above. The surface-dielectric function g of the multilayers was calculated with the continued-fraction formula (9) using isotropic dielectric functions described by (9). The relevant optical parameters of AlAs and GaAs are given in Table 1.

FK modes of a GaAs/AlAs superlattice exist in two frequencies regions defined by the ω_{TO} and ω_{LO} frequencies of both materials. These regions will be denoted by A and B for AlAs and GaAs, respectively. HREELS spectra of $(\text{GaAs}_3/\text{AlAs}_6)_p/\text{GaAs}(001)$ and $(\text{GaAs}_6/\text{AlAs}_6)_p/\text{GaAs}(001)$ superlattices are shown in Fig. 2 for $p = 1, 3, 6$, and 12 periods. The spectra obtained by the dielectric theory are represented by the solid lines. The dots are experimental data. The intensity of the

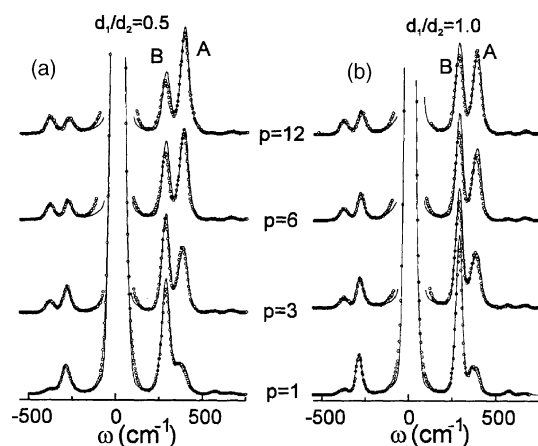


Fig. 2. HREELS spectra of (a) $(\text{GaAs}_3/\text{AlAs}_6)_p/\text{GaAs}(001)$ and (b) $(\text{GaAs}_6/\text{AlAs}_6)_p/\text{GaAs}(001)$ for $p = 1, 3, 6$, and 12. Dots are experimental data obtained with 10-eV electrons in specular reflection at incidence angle of 55°. Structures marked A and B correspond to modes of AlAs and GaAs character, respectively.

structure *B* (GaAs-like modes) progressively decreases with increasing number of periods. At the same time, the amplitude of the *A* structure increases (AlAs-like modes).

The features of the HREELS spectra can be investigated in more detail by comparing the classical loss spectra $P_{cl}(\omega)$ of the multilayers for increasing values of the period p (Fig. 3). For small values of p , the thickness of the superlattice is small and the spectrum is dominated by a GaAs interface mode in the *B* region originating from the GaAs substrate, called the *I* mode in Fig. 3. In the *A* region, there are two peaks associated with interface modes of AlAs character. As the number of periods increases, the weight of the substrate *I* mode is reduced, which explains the progressive decrease of the amplitude of the *B* loss peak in Fig. 2. Concomitantly, the number of interfaces modes of both GaAs and AlAs characters increases, which is why the weight of the peak *A* in Fig. 2 increases. When p is large enough, the role of the substrate is negligible, and both *A* and *B* peaks originate from the superlattice. In Fig. 3, the amplitudes of the *B* and *A* peaks are roughly equal, when the thicknesses of the GaAs and AlAs layers coincide, whereas there is roughly a factor of 0.5 between them when $d_1/d_2 = 0.5$.

The fine structure of the classical loss spectrum represented in Fig. 3 is not reproduced in the experimental spectra, due to the finite resolution of the spectrometer. In order to understand the evolution of this fine structure versus the superlattice thickness, it is interesting to consider a superlattice composed of a infinite number of

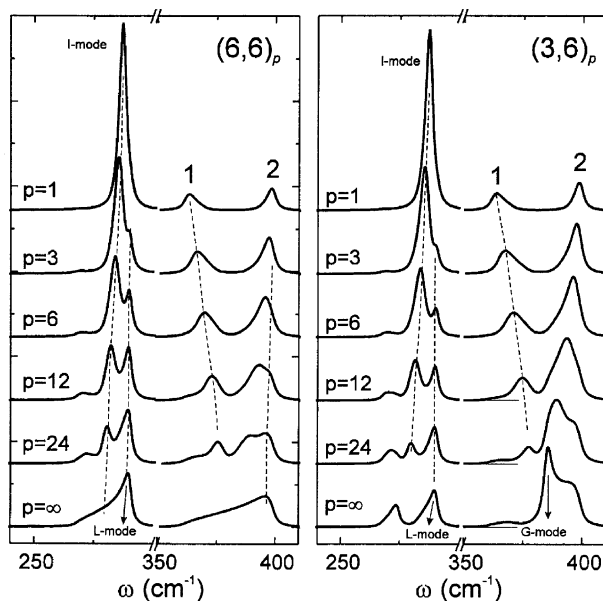


Fig. 3. Computed classical loss spectra of superlattices $(\text{GaAs}_3/\text{AlAs}_6)_p/\text{GaAs}(001)$ and $(\text{GaAs}_6/\text{AlAs}_6)_p/\text{GaAs}(001)$ for $p = 1, 3, 6, 12, 24$, and ∞ . *L* and *G* modes correspond to *L* and *G* branches in Fig. 4. *I* mode originates from thick GaAs substrate.

periods (limit $p \rightarrow \infty$). In this limiting case, the effective dielectric function ξ of the superlattice can be obtained analytically by computing the limit of the continued fraction (5). At this limit, ξ is the root of the quadratic equation

$$(a_1 + a_2)\xi^2 - (\epsilon_1^2 - \epsilon_2^2)\xi - (a_1\epsilon_2^2 + a_2\epsilon_1^2) = 0 \quad (10)$$

that is closest to the first approximation $a_1 - b_1^2/(a_1 + a_2)$ of the continued fraction [22]. For real ϵ 's, (10) possesses real and complex solutions. Complex solutions correspond to continua of FK modes in the (Q, ω) plane. These continua reflect the shape anisotropy of the superlattice. The continua can be viewed as formed by the accumulation of interfaces branches, when the number of layers approaches infinity [25]. They are represented by shaded areas in Fig. 4. Interestingly, a gap separates two continua of modes in both the *A* and *B* regions, except when the thicknesses d_1 and d_2 of the alternating layers coincide [22]. Discrete branches are found outside the continua, which are associated with real solutions of (10). They correspond to charge densities localized on the successive interfaces, whose amplitude decays exponentially, as one moves into the multilayer [26]. There is, in particular, a *L* branch localized above the continuum associated with the topmost layer (GaAs, region *B*). When $d_1 < d_2$, localized branches exist in the continuum gaps in both *A* and *B* regions (*G* modes). When $d_1 > d_2$, not examined here, there is only a short portion of the *G* branch in the gap of region *B*. All the features of the superlattice FK modes are discussed in [22]. One clearly sees in Fig. 3 how the classical spectrum of a finite superlattice approaches that of the infinite superlattice. The *L* and *G* branches give rise to well-defined peaks when $d_1 < d_2$. By comparison, the continua of modes lead to much broader contributions with small amplitudes. When $d_1 = d_2$, there remains but one localized branch, the *L* mode, with a clear asymmetric peak in the spectrum.

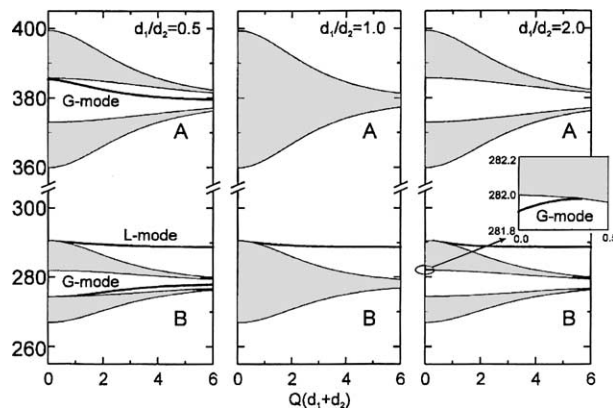


Fig. 4. FK modes of semi-infinite GaAs/AlAs superlattices for three ratios of layer thickness d_1 (GaAs, top layer) and d_2 (AlAs). Shaded areas correspond to continua of modes, solid-line curves are localized FK branches.

In Fig. 2, the intensity of the *B* structure, predicted by the dielectric theory, is slightly too large compared to experiment. This effect is due to the very small value of the thickness of the layers considered here. The same intensity disagreement already appears with just one thin AlAs layer on GaAs, such as in AlAs₄/GaAs, and disappears for thicker overlayers [27]. The fact is that the validity of the dielectric approximation is questionable for very thin layers. A careful analysis of the data in Fig. 2 also shows that the frequencies of the *A* and *B* peaks are slightly overestimated by the dielectric theory by a few cm⁻¹. The same effect has already been reported for very thin epitaxial layers of LiBr on Si(001) [28], and explained by microscopic lattice dynamics calculations [29]. The explanation is the following. Optical phonons of a GaAs/AlAs superlattice are confined within the layers [7,8], because they cannot propagate in the adjacent layers. There is a discrete number of optical modes in each layer, which form stationary waves with wavelength $\lambda = 2d/m$ with d the layer thickness and $m = 1, 2, \dots$. Here, the relevant thickness is $d = (n + 1)a_0/2$ with a_0 the fcc lattice parameter and n the number of atomic (001) planes in the layer. The frequencies of the confined modes can be approximately obtained from the bulk-phonon dispersion curve along the [001] direction, by discretizing the wave vector of the bulk phonons in the direction normal to the surface on a grid defined by $q_z = m2\pi/(n + 1)a_0$ [8], $m = 1, 2, \dots$. These confined modes all have frequencies lower than the LO and TO phonons computed at the Γ point, when the $\omega_{\text{LO}}(q_z)$ and $\omega_{\text{TO}}(q_z)$ branches disperse negatively in the direction normal to the surface, as is the case with GaAs and AlAs. Since the loss peaks in both *A* and *B* regions in Fig. 2 are weighted sums of the dielectric activities of all these confined phonons [21], the result is to shift down the position of the peaks with respect to the predictions of the dielectric theory [27]. This is so, because the dielectric functions, used in the calculation are based on the TO and LO frequencies at the Γ point ($q_z = 0$).

A correction to the dielectric theory can easily be obtained by computing the principal components of the dielectric tensor of an infinite superlattice with lattice dynamics. The microscopic calculation of the dielectric tensor of GaAs_{*n*}/AlAs_{*n*} ideal superlattices was performed with a shell model [27]. From an electrostatic point of view, a superlattice behaves like a uniaxial crystal due to its shape anisotropy. A semi-infinite superlattice can therefore be characterized by an effective dielectric function equal to the geometric mean of its two dielectric components ϵ_{\parallel} and ϵ_{\perp} , respectively parallel and perpendicular to the growth axis [30], $\xi = \sqrt{\epsilon_{\parallel}\epsilon_{\perp}}$. It is then easy to obtain the HREELS spectrum of a semi-infinite superlattice from (1). The results obtained are depicted in Fig. 5, where the positions of the *A* and *B* peaks obtained by this semi-microscopic approach are compared to the ones predicted by the continued fraction (5) when the bulk dielectric functions of GaAs and AlAs, computed with the same shell-model parameters as for the superlattice, are used. The loss peaks obtained with the semi-microscopic theory are shifted down with respect to those coming from the full dielectric theory, like in experiment. The fact that the loss peaks predicted by the dielectric theory have too high frequencies compared to experiment is therefore an indication of the loss of validity of the dielectric approximation when applied to very thin layers, as expected. This is due to the confinement of the phonons in the layers, as explained above.

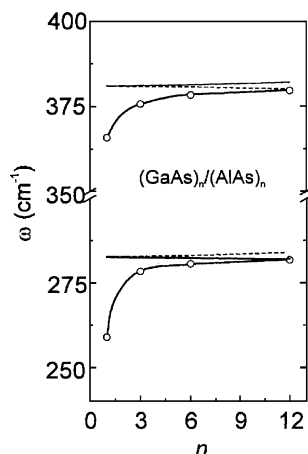


Fig. 5. Positions of AlAs and GaAs loss peaks in semi-infinite $\text{GaAs}_n/\text{AlAs}_n$ superlattices as a function of the number n of atomic planes in each layer. Full line with open circles is based on shell-model dynamics calculation of the superlattice dielectric tensor. Other curves are results predicted by full dielectric theory when using the bulk dielectric functions of AlAs and GaAs for a superlattice terminated with AlAs (solid line) and GaAs (dashed line).

Acknowledgements

The authors are grateful to J.L. Longueville for providing the experimental spectra of Fig. 1 and A.A. Lucas for helpful discussions. This work was performed in the framework of the Interuniversity Research Program IUAP P5/01 “Quantum size effects in nanostructured materials” of the Belgian OSTC.

References

- [1] L. Esaki, IEEE J. Quantum Elect. 22 (1986) 1611.
- [2] C. Weisbuch, J. Cryst. Growth 127 (1993) 742.
- [3] For a recent review on applications of semiconductor superlattices, see Z.I. Alferov, Semiconductors 32 (1998) 1.
- [4] Ph. Lambin, J.P. Vigneron, A.A. Lucas, P.A. Thiry, M. Liehr, J.J. Pireaux, R. Caudano, T.J. Kuech, Phys. Rev. Lett. 56 (1986) 1842.
- [5] A.A. Lucas, M. Sunjic, Phys. Rev. Lett. 26 (1971) 229.
- [6] L.J. Schowalter, R.W. Fathauer, R.P. Goehner, L.G. Turner, R.W. DeBlois, S. Hashimoto, J.L. Peng, W.M. Gibson, J.P. Krusius, J. Appl. Phys. 58 (1985) 302.
- [7] B. Jusserand, D. Paquet, Phys. Rev. Lett. 56 (1986) 1752.
- [8] S. Baroni, P. Giannozzi, E. Molinari, Phys. Rev. B 41 (1990) 3870.
- [9] H. Ibach, Phys. Rev. Lett. 24 (1971) 1416.
- [10] H. Ibach, D.L. Mills, Electron Energy Loss Spectroscopy and Surface Vibrations, Academic Press, New York, 1982.
- [11] Z. Penzar, M. Sunjic, Phys. Scripta 30 (1984) 431.
- [12] See e.g. B.N.J. Persson, J.E. Demuth, Phys. Rev. B 30 (1984) 5968.
- [13] H. Froitzheim, in: H. Ibach (Ed.), Electron Spectroscopy for Surface Analysis, Springer-Verlag, Berlin, 1977, pp. 205–246.

- [14] M. Sunjic, A.A. Lucas, *Phys. Rev. B* 3 (1971) 719.
- [15] R. Fuchs, K.L. Kliewer, *Phys. Rev.* 140 (1965) A2076.
- [16] E. Evans, D.L. Mills, *Phys. Rev. B* 7 (1973) 853.
- [17] D.L. Mills, *Surf. Sci.* 158 (1985) 411.
- [18] Ph. Lambin, J.P. Vigneron, A.A. Lucas, *Comput. Phys. Comm.* 60 (1990) 351.
- [19] W.L. Schaich, *Surf. Sci.* 122 (1982) 175.
- [20] See, e.g. A. Liebsch, *Phys. Scripta* 35 (1987) 354.
- [21] Ph. Lambin, P. Senet, A.A. Lucas, *Phys. Rev. B* 44 (1991) 6416.
- [22] Ph. Lambin, J.P. Vigneron, A.A. Lucas, *Phys. Rev. B* 32 (1985) 8203.
- [23] See, e.g. W.L. Schaich, *Phys. Rev. B* 24 (1981) 686.
- [24] M. Liehr, P.A. Thiry, J.J. Pireaux, R. Caudano, *Phys. Rev. B* 34 (1986) 7471.
- [25] Ph. Lambin, J.P. Vigneron, A.A. Lucas, *J. Elect. Spect. Rel. Phen.* 39 (1986) 59.
- [26] R.E. Camley, D.L. Mills, *Phys. Rev. B* 29 (1984) 1695.
- [27] J.L. Guyaux, M.D. Lange, R. Sporken, P.A. Thiry, R. Caudano, P. Senet, Ph. Lambin, *Surf. Sci.* 328 (1995) L566.
- [28] W. Gao, Y. Fujikawa, K. Saiki, A. Koma, *Solid State Commun.* 87 (1993) 1013.
- [29] P. Senet, Ph. Lambin, A.A. Lucas, *Phys. Rev. Lett.* 74 (1995) 570.
- [30] A.A. Lucas, J.P. Vigneron, *Solid State Commun.* 49 (1984) 327.